Nanostructured Pure Anatase Titania Tubes Replicated from Electrospun Polymer Fiber Templates by Atomic Layer Deposition

G.-M. Kim,*,† S.-M. Lee,‡ G. H. Michler,† H. Roggendorf,† U. Gösele,‡ and M. Knez‡

Institute of Physics, Martin-Luther-University, Halle-Wittenberg, D-06099 Halle/S., Germany, and Max Planck Institute of Microstructure Physics, D-06120 Halle/S., Germany

Received November 29, 2007. Revised Manuscript Received January 24, 2008

Pure anatase TiO_2 submicrotubes were successfully fabricated by a template-directed method. Electrospun poly(vinyl pyrrolidone) (PVP) fibers were used as a soft template for coating with titanium dioxide using an atomic layer deposition (ALD) technique. The deposition was conducted onto a template at 70 °C by using titanium tetraisopropyl oxide (TIP) [$Ti(O^iPr)_4$] and pure water as precursors of TiO_2. Crystalline structure, microstructure, and optical properties of the TiO_2 deposited layers before and after calcination were studied in detail. While the as-deposited TiO_2 layers onto ES fibers were completely amorphous with thickness of about 60 nm, the TiO_2 layers after calcination at 500 °C for 4 h were properly converted into polycrystalline nanostructured TiO_2 submicrotubes with high quality of anatase. Thereby, the optical band gap energy was also tuned with a blue shift. As final products the self-supported free-standing mats consisting of pure anatase TiO_2 submicrotubes can be easily handled and reclaimed for use in future applications related to catalysis, electronics, photonics, sensing, medicine, and controlled drug release.

1. Introduction

Titanium dioxide (TiO_2), also known as titania, is a versatile transition-metal oxide, both as particulate and thin film form, with a wide range of applications including solar cells,[1] photocatalysts[2] for air and water purification, high permittivity dielectric layers for electronic devices,[3] sensors for gas and biomolecules,[4] and biocompatible coatings for biomaterials.[5] TiO_2 occurs in nature in three distinct crystallographic phases: anatase, brookite, and rutile. Within these polymorphs, TiO_2 in the anatase phase has been proven to exhibit an excellent photocatalyst for photodecomposition and solar energy conversion due to its high photoactivity. It is of note that its physicochemical properties strongly depend on specific surfaces, crystallinity and crystal growth orientation. In the past decade, to further improve the properties of TiO_2 and to expand potential applications low-dimensional TiO_2 nanostructures with controllable crystalline phases, such as nanoparticles, nanofibers, nanostructured thin films or coatings and nanotubes, have been extensively studied, because they exhibit, in general, superior physical properties compared with conventional bulk materials. These unique properties mainly arise from the quantum-confinement effects and their enormous large specific areas.[6] In particular, TiO_2 microtubes with precisely defined nanoscale walls in high quality of crystal structure have attracted considerable attention due to the particularity of their structure.

Many procedures have been reported for the preparation of tubular structure from a wide range of materials, including self-assembly,[7] replica process,[8] chemical process[9] and template approach.[10] Among those processes, the template-directed approach is a most commonly applied strategy for fabricating inorganic micro and nanotubes due to its simple and easy processing, even at low temperatures. Among this line, alumina porous membrane,[6,11] colloidal particles,[12] inorganic and organic crystals nanorods,[13] carbon nanotubes[14] as well as natural materials including cotton and

* Corresponding author: gyeong.kim@physik.uni-halle.de (e-mail); +49 3461 46 2571(tel.); and +49 3461 46 2535 (fax).
† Martin-Luther-University.
‡ Max Planck Institute of Microstructure Physics.

(1) (a) O'Regan, B.; Grazel, M. *Nature* **1991**, *353*, 737. (b) Adachi, M.; Murata, Y.; Takao, J.; Jiu, J.; Sakamoto, M.; Wang, F. *J. Am. Chem. Soc.* **2004**, *126*, 14943. (c) Bach, U.; Lupo, D.; Comte, P.; Moser, J. E.; Weissörtel, F.; Salbeck, J.; Spretzer, H.; Grätzel, M. *Nature* **1998**, *395*, 583.
(2) (a) Fujishima, A.; Honda, K. *Nature* **1972**, *238*, 37. (b) Pore, V.; Rahtu, A.; Leskel, M.; Ritala, M.; Sajavaara, T.; Keinonen, J. *Chem. Vap. Deposition* **2004**, *10*, 143. (c) Mills, A.; Hunte, S. *J. Photochem. Photobiol., A* **1997**, *108*, 1.
(3) Campbell, S. A.; Kim, H. S.; Gilmer, D. C.; He, B.; Ma, T.; Gladfelter, W. L. *IBM J. Res. Dev.* **1999**, *34*, 383.
(4) Wang, R.; Hashimoto, K.; Fujishima, A.; Chikuni, M.; Kojima, E.; Kitamura, A.; Shimohigoshi, M.; Watanabe, T. *Nature* **1997**, *388*, 431.
(5) Huang, S. G.; Wu, X. L.; Kong, F.; Cheng, Y. C.; Siu, G. G.; Chu, P. K. *Appl. Phys. Lett.* **2006**, *89*, 073114.
(6) Hoffmann, M. R.; Martin, S. T.; Choi, W.; Bahnemann, D. W. *Chem. Rev.* **1995**, *95*, 69.
(7) Kobayashi, S.; Hanabusa, K.; Hamasaki, N.; Kimura, M.; Shirai, H. *Chem. Mater.* **2000**, *12*, 1523.
(8) Caroso, R. A. *Angew. Chem., Int. Ed.* **2004**, *43*, 2746.
(9) Kasuga, T.; Hiramatsu, M.; Hoson, A.; Sekino, T.; Niihara, K. *Adv. Mater.* **1999**, *11*, 1307.
(10) (a) Martin, C. R. *Science* **1994**, *266*, 1961. (b) Hulteen, J. C.; Jirage, K. B.; Martin, C. R. *J. Am. Chem. Soc.* **1998**, *120*, 6603. (c) Caruso, R. A.; Schattka, J. H.; Greiner, A. *Adv. Mater.* **2001**, *13*, 1577.
(11) Lakshmi, B. B.; Dorhout, P. K.; Martin, C. R. *Chem. Mater.* **1997**, *9*, 857.
(12) Rugge, A.; Becker, J. S.; Gordon, R. G.; Sarah, H.; Tolbert, S. H. *Nano Lett.* **2003**, *3*, 1293.
(13) Lauhon, L. J.; Gudiksen, M. S.; Wang, C. L.; Lieber, C. M. *Nature* **2002**, *420*, 57.
(14) (a) Satishkumar, B. C.; Govindaraj, A.; Nath, M.; Rao, C. N. R. *J. Mater. Chem.* **2000**, *10*, 2115. (b) Min, Y. S.; Bae, E. J.; Jeong, K. S.; Cho, Y. J.; Lee, J. H.; Choi, W. B.; Park, G. S. *Adv. Mater.* **2003**, *15*, 1019.

10.1021/cm703398b CCC: $40.75
Published on Web 04/10/2008

paper[15] have been often used as templates. Among them, 1-dimensional nanostructures are more useful as templates to fabricate nanotubes of various materials.[16]

To fabricate 1-D nanostructures to be used as template the electrospinning (ES) process has been already proven to be a powerful technique, achieving fiber diameters from micrometer to nanometer scales straightforwardly and cost-effectively. The resulting fibers are, in general, continuous (and thus possess an extremely high aspect ratio) and have a large specific surface area (and thus strongly interacte with the environment). In a typical process, a polymer solution (or melt) is forced through a capillary, forming a drop of polymer solution at the tip of capillary. Then a high voltage is applied between the tip and a grounded collection target. When the electric field strength overcomes the surface tension of the droplet, a polymer solution jet forms and is accelerated toward the collection target. As the jet travels through the air, the solvent evaporates and a nonwoven polymeric fabric is formed on the target within a period of time as short as a few seconds. By careful peeling off from the collector one obtains free-standing mats consisted of ES-fibers for use as templates for further experimental procedures.

Atomic layer deposition (ALD)[17] is a self-limiting process, which relies on a sequential surface chemistry that deposits conformal thin films of materials onto substrates of varying compositions. ALD is a modified chemical vapor deposition (CVD) technique, except that the ALD reaction separates the CVD reaction into two half-reactions, keeping the precursor materials separate during the reaction. ALD film growth relies on the sequential self-limiting surface reactions, which facilitates a highly reproducible growth of extremely uniform inorganic layers with atomic scale thicknesses. Depending on the process, deposited films can be amorphous, single crystalline or polycrystalline. ALD has unique advantages over other thin film deposition techniques: ALD grown films are superior in uniformity and conformality, being pinhole free and having low impurities content, and are chemically bonded to the substrate. Additionally, in some cases ALD can be performed at relatively low temperatures (<100 °C), well below typical CVD temperatures, thus reducing thermal damage to temperature-sensitive substrates such as bioorganic species, organic media and polymers.[18] As a consequence, during the past decade ALD has attracted considerable attention as a unique method of manufacturing conformal inorganic material films in high-quality over large areas on the complex, 3-dimensional substrates with severe topography, including for example, deep trenches and tortuous porous networks.

In this work we demonstrate an effective and robust strategy for fabricating long and uniform TiO_2 submicrotubes with a precisely controlled wall thickness on the nanometer scale. The processing mainly comprised three steps; first, the fabrication of polymeric fibers by electrospinning to be used as templates[19] and then the deposition of TiO_2 onto the ES-fibers by ALD. It is emphasized here that the chemical reactions in ALD process strongly depend on the specific reactive functional groups present on the surface prior to the deposition. Thus, the advantage of using poly(vinyl pyrrolidone) (PVP) ES-fibers as the template compared to other species is that the molecules contain functional groups that can react directly with the ALD precursors without any surface modification. As a last step, calcination was applied in order to remove the inner electrospun fibers by decomposition and to simultaneously achieve TiO_2 thin film with high quality crystalline anatase. Detailed structural properties, including the tube diameter, wall thickness, and crystal structure as well as optical properties, i.e., optical band gap energy of the TiO_2 tubes are discussed. The capability and feasibility of the technique presented in this work provides a promising alternative approach for the fabrication of high-quality templated microtubes in widespread future applications related, but not limited, to catalysis, electronics, photonics, sensing, medicine and controlled drug release.

2. Experimental Section

2.1. Electrospinning of Template. PVP (molecular weight of 360 kDa) was purchased from Sigma Aldrich and used without further treatment or purification. To obtain electrospinnable solutions, PVP was dissolved in deionized water (DI H_2O) at room temperature to prepare 15 wt % solutions. These solutions were vigorously stirred with a magnetic stir bar for at least 24 h at room temperature to ensure homogeneity. Electrospinning was carried out at room temperature in a vertical spinning configuration, using a 1 mm inner diameter flat-end needle with an 8 cm working distance and a flow rate of 0.1 mL/h. The applied voltages were in the range from 3 to 20 kV, driven by a high voltage power supply (Knürr-Heizinger PNC, Germany). The electrospun fibers were collected directly on the grounded aluminum foil. To get the free-standing templates the deposited nonwoven ES-fibers were carefully peeled out from aluminum foils for further ALD.

2.2. Preparation of TiO_2 Thin Films by ALD and TiO_2 Tubes by Calcination. The predried ES-fiber mats as templates were transferred into an ALD chamber (Savannah 100, Cambridge Nanotechnology Inc.) and evacuated at 1×10^{-1} Torr at 35 °C for 2 h in order to remove remaining loosely bound water from the template. The TiO_2 thin films were deposited onto the nonwoven ES-fiber mats using titanium tetraisopropyl oxide (TIP) $[Ti(O^iPr)_4]$ from Sigma Aldrich and water as ALD precursors. Ar gas served as both a carrier and a purging gas. Pulsing times were 1.5 and 1.3 s for TIP and water, respectively. Exposure and purging times of 30 s were used for all pulses. The total flow rate of the Ar purging was 20 sccm. Each cycle for TiO_2 deposition consisted of a TIP exposure, an Ar purge, a H_2O exposure, and a second Ar purge. The total deposition for TiO_2 thin films onto the templates was conducted by 1000 cycles at 70 °C under 1×10^{-2} Torr.

(15) Kemell, M.; Pore, V.; Ritala, M.; Leskela, M.; Linden, M. *J. Am. Chem. Soc.* **2005**, *127*, 14178.
(16) (a) Rao, C. N. R.; Govindaraj, A. *Nanotubes and Nanowires*; Royal Society of Chemistry: Cambridge, 2005. (b) Rao, C. N. R.; Müller, A.; Cheetham, A. *The Chemistry of Nanomaterials. Synthesis, Properties and Applications*, 2nd ed.; Wiley-VCH: Weinheim, 2004. (c) Sun, Y.; Mayers, B. T.; Xia, Y. *Nano Lett.* **2002**, *2*, 481.
(17) Ritala, M.; Leskela, M. In *Handbook of Thin Film Materials*; Nalwa, H. S., Ed.; Academic Press: San Diego, CA, 2002; Vol. 1, pp 103−159.
(18) (a) Knez, M.; Kadri, A.; Wege, C.; Gösele, U.; Holger Jeske, H.; Nielsch, K. *Nano Lett.* **2006**, *6*, 1172. (b) Groner, M. D.; Fabreguette, F. H.; Elam, J. W.; George, S. M. *Chem. Mater.* **2004**, *16*, 639–645.
(19) (a) Peng, G.; Sun, X.-Y.; Spagnola, J. C.; Hyde, G. K.; Spontak, R. J.; Parsons, G. N. *Nano Lett.* **2007**, *7*, 719. (b) Leskela, M.; Kemell, M.; Kukli, K.; Pore, V.; Santala, E.; Ritala, M.; Lu, J. *Mater. Sci. Eng., C* **2007**, *27*, 1504.

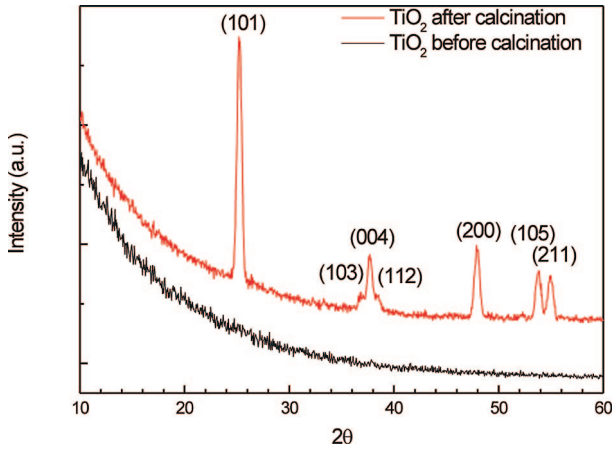

Figure 1. WAXS patterns of as-TiO_2 deposited ES-fibers before and after calcination at 500 °C for 4 h. The designated peak labels are the Miller indices corresponding to the crystal planes of calcined TiO_2. All diffraction peaks noted correspond to the anatase phase.

Calcination was then carried out to remove the template consisted of the ES PVP fibers in air at 500 °C for 4 h.

2.3. Characterization Techniques. To analyze the crystalline structure of the TiO_2 films, both as-deposited and after calcination, wide-angle X-ray scattering (WAXS) was performed with a Seifert XRD 3000 using Cu Kα radiation ($\lambda = 1.54056$ Å). The tube source was operated at 40 kV and 30 mA. Scans were run over a 2θ range of 10−60° with a step of 0.05° and a dwell time of 1 s. The size and morphology of the as-ES fibers, as-TiO_2 deposited ES-fibers and the calcined TiO_2 tubes were investigated by field emission gun environmental scanning electron microscopy (FEG-ESEM, Philips ESEM XL 30 FEG), conventional transmission electron microscopy (TEM) (JEOL 200CX operated at 200 kV) as well as by high-resolution TEM (Philips CM200 FEG\ST Lorentz electron microscope with a field emission gun and at an acceleration voltage of 200 kV). The diameter of the fibers and TiO_2 tubes, and their size distribution were analyzed by measuring over 200 fibers and tubes using randomly recorded FEG-ESEM micrographs, using an image analysis software (Analysis, Soft Imaging System Co., Germany). The optical transmission spectra were measured with a Perkin-Elmer Lambda 2S UV/vis spectrophotometer at room temperature in the wavelength range 200−800 nm.

3. Results and Discussion

3.1. Crystalline Structure of TiO_2. Figure 1 shows the XRD patterns of the as-deposited titania on the PVP ES-fibers by applying 1000 cycles of ALD and their calcined titania tubes. From the results, 2θ-values observed from XRD pattern of TiO_2 tubes, D-values determined from 2θ-values ($d_{2\theta}$) and the corresponding Miller indices (*hkl*) are summarized in Table 1. In order to facilitate better understanding of the results presented in this works the three most naturally occurring polymorphs of titania are listed as follows;[20] anatase (tetragonal, space group $I4_1/amd$, lattice parameters: $a = b = 0.378$ nm and $c = 0.951$ nm), rutile (tetragonal, space group $P4_2/mnm$, lattice parameters: $a = b = 0.459$ nm and $c = 0.296$ nm) and brookite (orthorhombic, space group *Pbca*, lattice parameters: $a = 0.92$ nm, $b = 0.547$ and $c = 0.517$ nm).

Table 1. 2θ Values Observed from the XRD Pattern of TiO_2 Tubes after Calcination, d-vValues Determined from 2θ-Values ($d_{2\theta}$), and Corresponding Indices (*hkl*) and the Calculated Lattice Parameters

2θ	$d_{2\theta}$ (nm)	*hkl*
25.24	0.3532	101
36.83	0.2438	103
37.73	0.2384	004
38.52	0.2332	112
48.00	0.1894	200
53.77	0.1699	105
54.93	0.1667	211

calculated lattice parameters: $c = 0.954$ nm; $a = 0.379$ nm

As can be clearly seen in Figure 1, for the as-deposited titania films on the electrospun PVP fibers prepared at 70 °C, there is no sign of any diffraction peaks, indicating that TiO_2 layer was predominantly amorphous. This kind of amorphous TiO_2 films are often observed when the substrate temperature during deposition is low.[21]

In contrast, after calcination at 500 °C in air for 4 h the remaining titania submicrometer tubes with well-defined wall thickness of about 60 nm (as discussed later) showed the characteristic peaks in the XRD pattern, indicating a high-quality polycrystalline nature of TiO_2, in which the reflex (101) is the most predominant. Their corresponding *d* spacings indicated that during calcination the amorphous titania layers highly crystallized in anatase crystalline phase (tetragonal D_{4h}, $I4_1/amd$).[22] Except for the anatase phase, no indication of other crystalline phases, such as rutile or brookite, could be identified in this diffractogram. This implies that the pure anatase phase could be easily formed at a calcination temperature of 500 °C.[23]

The crystal size of the polycrystalline TiO_2 tubes can be determined from the broadening of the corresponding X-ray spectral peaks from Scherrer's formula,

$$L = \frac{K\lambda}{B(2\theta)\cos\theta} \quad (1)$$

where *L* is the crystallite size, *K* is a constant taken as the default value of 0.89, λ is the wavelength of the X-ray, $B(2\theta)$ is the full width at the half-maximum intensity (fwhm), and θ is the Bragg angle. The width of the diffraction peak with the highest intensity (101) was selected for the calculation. The estimated crystallite size L of anatase TiO_2 tubes was ca. 16 nm

3.2. Microstructure of TiO_2. Besides confirming the anatase phase found by XRD, the morphology, surface structure and size of the as-ES fibers, the as-titania deposited fiber and the calcined taitania were characterized with SEM, TEM and HR-TEM. Figure 2a shows a representative SEM image of individual as-electrospun PVP fibers is presented in Figure 2a. As expected, the ES-fibers were typically connected each other to form a self-supporting web. The diameters of PVP ES-fibers are in a submicrometer range with an average fiber diameter of about 500 nm. The as-deposited TiO_2 films by ALD for 1000 cycles on the ES-

(20) Banfield, J. F.; Bischoff, B. L.; Anderson, M. A. *Chem. Geol.* **1993**, *110*, 211.
(21) Sander, M. S.; Cote, M. J.; Gu, W.; Kile, B. M.; Tripp, C. P. *Adv. Mater.* **204**, *16*, 2052.
(22) Joint Committee on Powder Diffraction Standards File, JCPDS 21-1272.
(23) Li, D.; Xia, Y. *Nano Lett.* **2003**, *3*, 555–560.

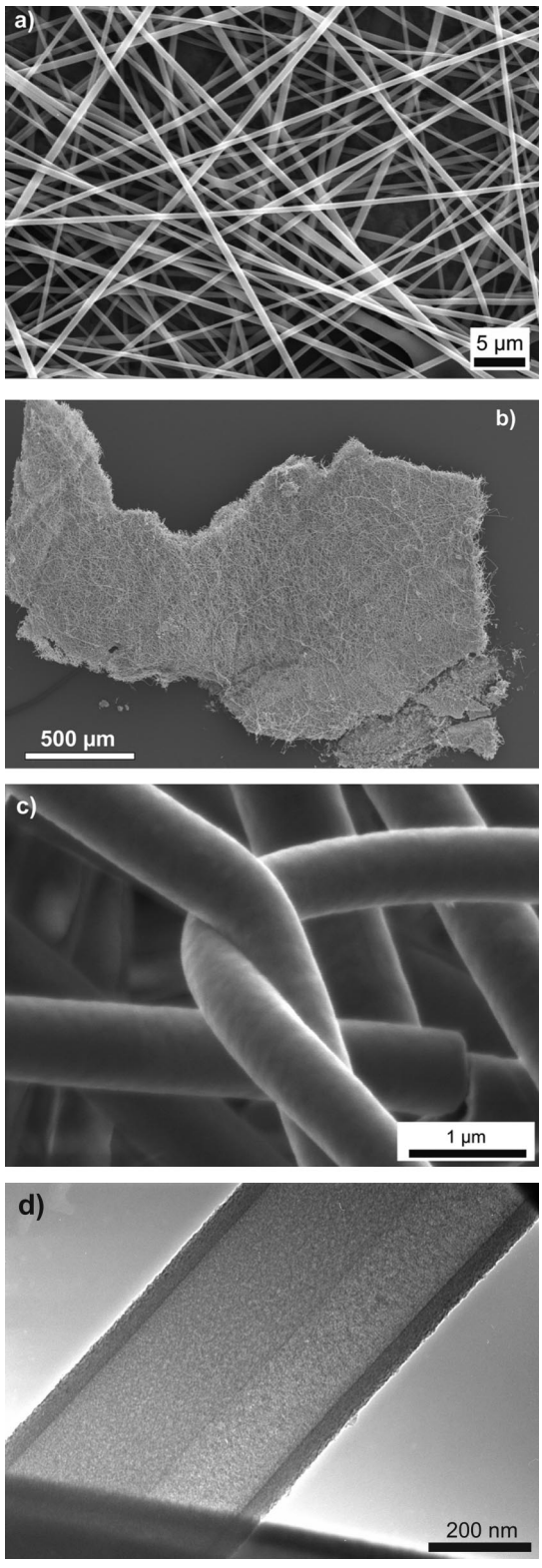

Figure 2. SEM micrographs (a) for as-ES fibers and (b and c) for as-TiO_2 deposited ES-fibers and TEM micrograph (d) for as-TiO_2 deposited ES-fibers.

fibers are shown in the SEM image displayed in Figure 2b,c, indicating that the TiO_2 microtubes are connected together in a web, thereby preserving the original arrangement of the PVP electrospun fiber templates. Figure 2d shows a TEM micrograph of single ES-fiber deposited TiO_2 in high magnification, demonstrating that the wall thickness of the microtubes is ~60 nm and is remarkably uniform along the

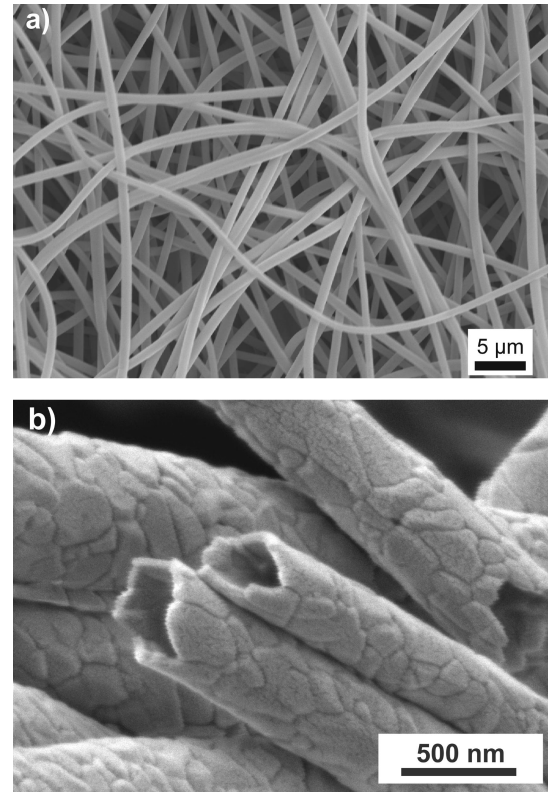

Figure 3. SEM micrographs (a) for TiO_2 tubes after calcination at 500 °C for 4 h and (b) for a close-up image from broken parts of the tubes.

length of a single tube. Based on the images from both SEM and TEM, it could be confirmed that the ALD process yields a uniform coverage and high conformality without any particularities such as the cracks and pin-holes over a relatively large area despite the apparent topological complexity.

Figure 3a is a SEM image of TiO_2 replica of PVP electrospun fibers that was first exposed to TiO_2 via ALD after 1000 cycles and then followed by calcination in air at 500 °C for 24 h to remove the PVP core. It is apparent in Figure 3a that the interconnection of tubes is still retained as in the as-ES PVP fiber template without cracking. It is worth noting that the removing process did not change the morphology and size of the tubes. The only difference was a minor distortion in their curvedness; The fibers in Figure 2a were dried in air at room temperature and appeared to be straight in SEM migragraphs, which were attributed to the fact that during drying the fibers were most likely fully stretched between the fiber junction points. In contrast, during in our ALD procedure the water was first exposed to the fibers consisting a hydrophilic PVP polymer, indicating that water can chemically react with such a hydrophilic polymer. This chemical reaction with water makes the PVP fibers flexible and thus induces the distortion in fiber curvedness.

The most striking occurrence on the surface morphology of TiO_2 microtubes after calcination is revealed in a close-up SEM image. As seen in Figure 3b, the wall of the calcined TiO_2 tubes primarily consists of the well-developed small platelet grains over the entire tubes with a high packing density. The platelets are most likely aligned along the tube axis but randomly distributed over the tubes with average grain size of about 10−250 nm in conjunction with wall

thickness estimated to be about 60 nm. This result indicates the polycrystalline character of the films, meaning that several domains with different atomic arrangements are aligned parallel to the axial direction of the tube. It is noted that the wall thickness is still preserved after calcination. In other words, the TiO_2 wall thickness is not significantly affected by heat treatment.

As confirmed by XRD measurements, the TiO_2 films were polycrystalline with platelet-like grains composed of well crystallized anatase TiO_2. The appearance of larger grains suggests that calcination is conductive to grain growth via dissolution-reprecipitation mechanism (i.e., Ostwald ripening) in which larger grains grow at the expense of smaller ones.[24]

Figure 4a shows a TEM image of the calcined titania tubes and the corresponding selected area electron diffraction (SAED) pattern. Despite their diameter (in excess of 200 nm), these microtubes appear to be electron transparent when observed by TEM. This TEM image clearly points out that the titania tubes consisted of platelet grains were uniform, homogeneous and without visible defects. The SAED pattern is shown as an inset in Figure 4a. The pattern displays obvious rings with diffuse spots, indicating that the TiO_2 films are polycrystalline,[25] consist of randomly oriented grains having the analyzed specimen volume.

To identify the crystalline phase of the grains HR-TEM was performed and the lattice fringes between parallel crystalline planes were rigorously checked during the HR-TEM analysis. The HR-TEM images (Figure 4b−d) were taken from the open end of a single titania tube (see Supporting Information). The plan-view image in Figure 4b clearly shows that well-defined grains and grain boundaries are displayed in the TiO_2 tubes. In the present work, the mean grain size (105 ± 65 nm) in polycrystalline titania tubes estimated from SEM and TEM analysis reveal a much larger and broader grain size distribution compared with those (16 ± 5 nm) calculated from the XRD results. This discrepancy between XRD and electron microscopic observations might be explained by following facts: at first, small angle grain boundaries do not show strong contrast in TEM images, while X-ray diffraction is affected by them. Indeed, considering the XRD results discussed above, the dimension of grain (defined as a crystallographically coherent area) was calculated from the highest intense peak while TEM and SEM gave the average value of the grain size. On the other hand, close inspection of the individual grains provides change in contrast fluctuation (see Figure 4b), which may indicate the presence of smaller subdomains or coherent areas within the grains.

Figure 4c is a HR-TEM image of grains where the close-packed grains and the neat surface of the discrete crystallites were apparent. The detailed image obviously revealed the presence of two types of crystalline grains, as characterized by their difference in the direction of growth (Figure 4d). The corresponding lattice fringes parallel to the surface marked in the top left corner (1) and the bottom right corner

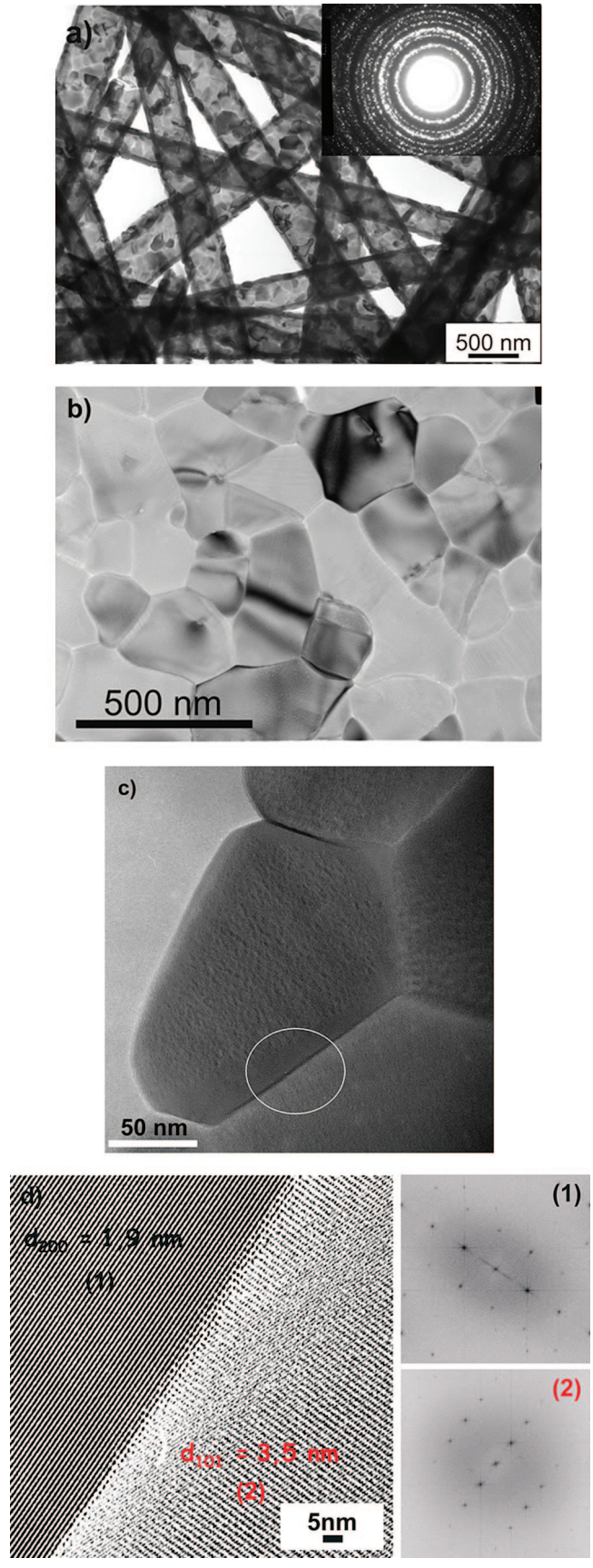

Figure 4. (a) Bright field TEM image of several titania tubes after calcination (the SAED pattern as inset), (b) plan-view HR-TEM image taken from at the open end of a single titania tube, (c) HR-TEM image of grains in high magnification of (b), and (d) HR-TEM image taken from the circle in (c), including the lattice fringes in the (101) and (200) direction.

(24) Yu, J.; Guo, H.; Davis, S. A.; Mann, S. *Adv. Funct. Mater.* **2006**, *16*, 2035.
(25) Mugnier, J.; Varrel, B.; Bahtat, M.; Bovier, C.; Serughetti, J. *J. Mater. Sci. Lett.* **1992**, *11*, 875.

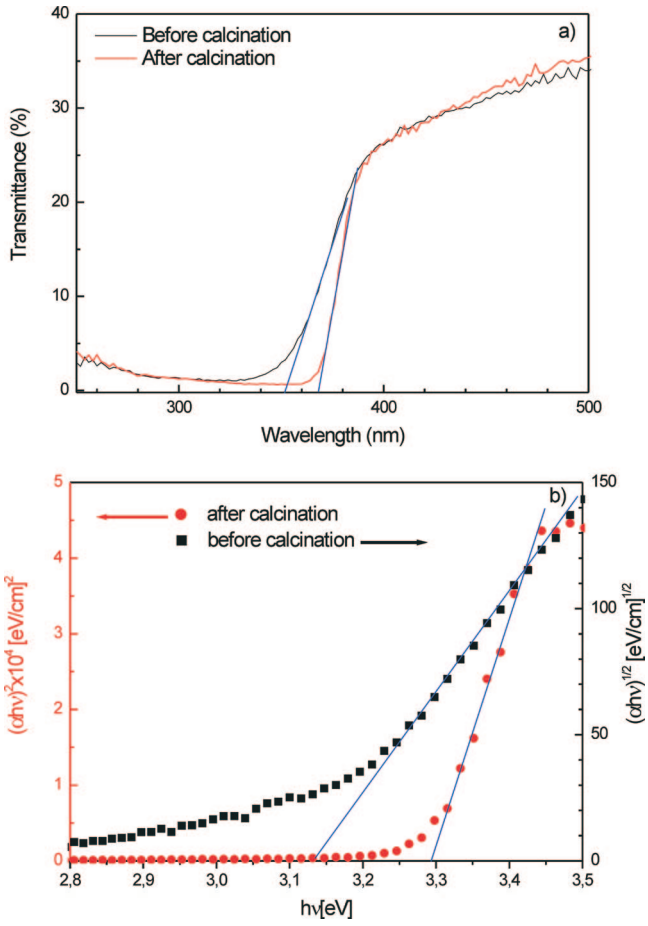

Figure 5. (a) Transmittance versus wavelength spectra and (b) the dependence of $(\alpha h\nu)^2$ for and $(\alpha h\nu)^{1/2}$ on the photon energy ($h\nu$) for as-TiO_2 deposited ES-fibers and calcined TiO_2 tubes at 500 °C for 4 h.

(2) could be readily resolved and estimated to be 0.35 and 0.19 nm, respectively. These values are in good agreement with the (101) and (200) planes of anatase crystal structure in TiO_2 as confirmed by XRD measurements, respectively. Thus, combined with the XRD data and HR-TEM images, such features imply that the platelet anatase grains grew preferentially along the [101] and [200] direction parallel to the axial direction of the tube upon calcination process (see FFT images in Figure 4d). It is worth noting again that in conjunction with XRD measurements no other lattice fringes were detected in the whole HR-TEM analysis. Conclusively, the grains on the calcined TiO_2 tubes are confirmed to be purely nanocrystalline single-phase anatase.

3.3. Optical Property: Energy Band Gap of TiO_2 Submicrometer Tubes. The analysis of optical absorption spectra is one of the most practical tools for understanding and developing the band structure and energy gap of both crystalline and amorphous semiconducting materials. To this end, we performed optical measurements in the UV−visible range from 100 to 800 nm wavelength by a Perkin-Elmer Lambda 2S UV/vis spectrometer in order to obtain clues regarding the band gap energy of the TiO_2 films.

Figure 5a shows typical UV−visible transmittance spectra in the wavelength range of 250−500 nm for the as-TiO_2 deposited PVP fibers (black line) together with the polycrystalline anatase TiO_2 tubes (red line). Both films were highly transparent to light for wavelengths longer than about 430 nm. At the wavelength of 500 nm, the films showed a transmittance of 35%, and at a wavelength of 300 nm the films transmitted practically the whole light which came in.[26] As the wavelength of the light decreased, the transmittance in both systems before and after calcination of TiO_2 also decreased. The sharp decrease in the transparency of the TiO_2 tubes in the UV region results from the fundamental light absorption of the semiconductor.

The onset of transmittance was obtained by extrapolating the steep part of the rising transmittance curve. The onset transmittance of TiO_2/PVP before and after calcination appears at λ_{onset} = 350.5 and 370.0 nm, respectively, indicating that the calcination leads to a blue shift of the onset of transmittance. In addition, the slope of extrapolated line for the amorphous TiO_2 is relatively lower than that of polycrystalline TiO_2 due to a broadening of states because of the disordered structure of the films and to the presence of exponentially distributed states below the absorption edge extending into the gap of the film.

The effective band gap as derived from the transmittance spectra is by definition the energy necessary to create an electron (e-) and hole (h+) pair. In principle, the excited electron−hole pair forms a bound state, i.e., Wannier excition, and the behavior of the exciton may be calculated using a "confined exciton" model which gives an increase in the apparent band gap energy. In semiconductor physics, the general expression that relates the absorption coefficient to the energy band gap is given by

$$(\alpha h\nu)^m = h\nu - E_g \qquad (2)$$

where m is an index that can assume values of (1/2, 2) depending on the nature of the electronic transitions, α is the absorption coefficient, h is the Planck constant, $h\nu$ is the energy of the electromagnetic radiation, and E_g is band gap energy, i.e., the energy of the involved quantum levels in the semiconductor.[25,27] It should be noted here that when m = 2, the semiconductor has a direct band gap, and under electromagnetic excitation, the electron executes a direct allowed transition from the valence to the conduction band, while when m = 1/2, the semiconductor has an indirect band gap and the transitions are indirectly allowed.

To estimate band gap energies of these films, α data in Figure 5a are replotted on $(\alpha h\nu)^2$ for polycrystalline TiO_2 and on $(\alpha h\nu)^{1/2}$ for amorphous TiO_2 as a function of the photon energy $h\nu$ in Figure 5b. That is, the absorption edge of TiO_2 is assumed to be a direct transition for polycrystalline TiO_2 and the Tauc's plot is employed for amorphous TiO_2. The band gap energies were determined by the extrapolation of best fit lines using a graphic presentation of $(\alpha h\nu)^m = f(h\nu)$ to intercept with the phonon energy ($h\nu$) axis. Noted hereby that the measured transmittance T was converted into absorption coefficient α, using the relationship given by

(26) Johson, J. B.; Jones, H.; Latham, B. S.; Parker, J. D.; Engelken Barber, R. D.; Semicond, C. *Sci. Technol.* **1999**, *14*, 501.
(27) (a) Tauc, J. *Amorphous and Liquid Semiconductor*; Plenum Press; New York, 1974. (b) Callaway, J. *Quantum Theory of the Solid State*; Academic: New York, 1974; p 516. (c) Linsebigler, A. L.; Lu, G.; Yates, J. T., Jr. *Chem. Rev.* **1995**, *95*, 735.

$$\alpha = \frac{\ln\left(\frac{100}{T(\%)}\right)}{d} \quad (3)$$

where T is transmittance and d is thickness of the film.[26]

From Figure 5b the E_g for polycrystalline TiO_2, obtained by dropping a line from the maximum slope of the curve to the $h\nu$-axis, is 3.29 eV. This is slightly larger than the commonly reported band gap energy (E_g = 3.23 eV, λ = 385 nm) for TiO_2 anatase phase.[28] This increase in E_g, i.e, a blue shift is most likely arisen from the quantum-confinement of TiO_2 wall thickness.[29] In general, a film consisting of fine crystallites shows this kind of blue shift [39]. One other possible explanation for this effect is that the difference of band gap energies between the well-crystallized films and the single crystals arises from the existence of grain boundaries in the polycrystalline thin films. The atomic structure at the grain boundary is different from that in the grain, which leads to larger free carrier concentrations and the existence of potential barriers at the boundaries. Therefore, an electric field is formed, the band gap energy increases, and the absorption limit shifts to shorter wavelengths.

In contrast, when indirectly allowed transition for TiO_2 is taken into account, shown as black curve in Figure 5b for a $(\alpha h\nu)^{1/2}$ versus $h\nu$, a small diminution in the indirect band gap value of 3.13 eV is found. It is plausible that the band gap energy of amorphous materials becomes a lower value than that of crystalline phase in the direct band gap material because the density of state diffuses to the lower energy state by the introducing of structural disorder. Based on the results from Figure 5b a calculation of the UV absorption edges of the TiO_2 films returns a value of λ_0= 377 and 396 nm for direct and indirect band gap, respectively.

In conclusion, the crystallinity and functional properties of ALD-derived oxide thin films strongly depend on heat treatment,[30] this may allow adjustment of optical properties, even tailoring the band gap energies of the thin films by heat treatment and film thickness, and correspondingly, changing film cystallinity. It is believed that the dependence of the band gap energies of the thin films on film thickness should find applications in integrated optical devices.

4. Conclusions

An effective fabrication of long, uniform free-standing TiO_2 submicrotubes consisted of pure anatase phase with well controllable thickness by using ALD was presented in this work. The as-deposited TiO_2 onto ES-fibers as a template by ALD at 70 °C using precursors of titanium isopropoxide and water were amorphous in nature. After calcination at 500 °C for 4 h the amorphous TiO_2 preferentially developed into anatase crystalline platelet grains in a range of about 16 nm parallel to the direction of the tube axis, sequentially the polycrystalline nanostructured pure anatase TiO_2 tubes were obtained. The resulting TiO_2 submicrotubes were proven to be photosemiconducting with a band gap of about 3.29 eV. Due to their tunable band gap energy and ultrahigh specific surface areas, well-developed porosity as well as unique structural particularity the free-standing, self-supporting TiO_2 tubular mats makes it suitable for advanced materials applications.

Acknowledgment. S.-M.L., M.K., and U.G. greatly acknowledge the financial support by the German Ministry of Eucation and Research under Contract No. FKZ03X557. We greatly acknowledge Dr. Scholz for assistance in HR-TEM investigation.

Supporting Information Available: TEM image taken from the open end of the single calcined TiO_2 tube. This material is available free of charge via the Internet at http://pubs.acs.org.

CM703398B

(28) (a) Bao, D. H.; Gu, H. S.; Kuang, A. X. *Thin Solid Films* **1998**, *312*, 37. (b) Consadori, F.; Frindt, R. F. *Phys. Rev. B2* **1970**, 4893.
(29) Wang, Y.; Herron, N. *J. Phys. Chem.* **1991**, *95*, 525.
(30) Bao, D. H.; Mizutani, N.; Zhang, L. Y.; Yao, X. J. *Appl. Phys.* **2001**, *89*, 801.